NEURAL REGENERATION RESEARCH
www.nrronline.org

Research Article

The ferroptosis activity is associated with neurological recovery following chronic compressive spinal cord injury

Zhengran Yu[1, #], Xing Cheng[2, #], Wenxu Pan[3, #], Cheng Yu[4], Yang Duan[4, *]

https://doi.org/10.4103/1673-5374.371378
Date of submission: October 8, 2022
Date of decision: January 4, 2023
Date of acceptance: February 6, 2023
Date of web publication: March 15, 2023

From the Contents

Graphical Abstract

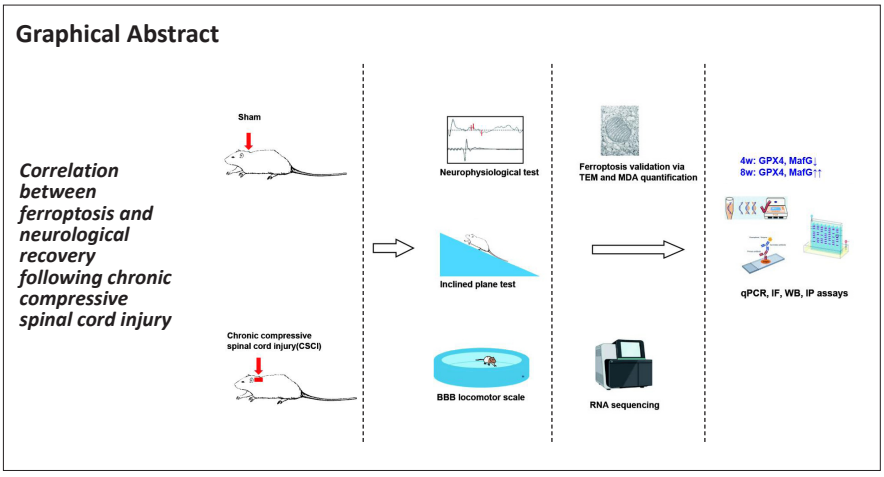

Abstract

Chronic compressive spinal cord injury in compressive cervical myelopathy conditions can lead to rapid neurological deterioration in the early phase, followed by partial self-recovery, and ultimately an equilibrium state of neurological dysfunction. Ferroptosis is a crucial pathological process in many neurodegenerative diseases; however, its role in chronic compressive spinal cord injury remains unclear. In this study, we established a chronic compressive spinal cord injury rat model, which displayed its most severe behavioral and electrophysiological dysfunction at 4 weeks and partial recovery at 8 weeks after compression. Bulk RNA sequencing data identified enriched functional pathways, including ferroptosis, presynapse, and postsynaptic membrane activity at both 4 and 8 weeks following chronic compressive spinal cord injury. Transmission electron microscopy and malondialdehyde quantification assay confirmed that ferroptosis activity peaked at 4 weeks and was attenuated at 8 weeks after chronic compression. Ferroptosis activity was negatively correlated with behavioral score. Immunofluorescence, quantitative polymerase chain reaction, and western blotting showed that expression of the anti-ferroptosis molecules, glutathione peroxidase 4 (GPX4) and MAF BZIP transcription factor G (MafG), in neurons was suppressed at 4 weeks and upregulated at 8 weeks following spinal cord compression. There was a positive correlation between the expression of these two molecules, suggesting that they may work together to contribute to functional recovery following chronic compressive spinal cord injury. In conclusion, our study determined the genome-wide expression profile and ferroptosis activity of a consistently compressed spinal cord at different time points. The results showed that anti-ferroptosis genes, specifically *GPX4* and *MafG*, may be involved in spontaneous neurological recovery at 8 weeks of chronic compressive spinal cord injury. These findings contribute to a better understanding of the mechanisms underlying chronic compressive spinal cord injury and may help identify new therapeutic targets for compressive cervical myelopathy.

Key Words: chronic spinal cord compression; compressive cervical myelopathy; ferroptosis; genome-wide transcriptome; glutathione peroxidase 4 (GPX4); MAF BZIP transcription factor G (MafG); neurological function

Introduction

Chronic cervical compressive spinal cord injury (CSCI) is a prevalent pathological condition that can lead to compressive cervical myelopathy (CCM). Many different conditions, such as cervical disc herniation, ossification of the posterior longitudinal ligament, and intraspinal tumors, can lead to chronic CSCI, which causes neurological dysfunction and can seriously affect a patient's quality of life (Badhiwala et al., 2020). In recent years, a lot of effort has been made to establish consistent spinal cord compression in different animal models, including by inducing intraspinal tumors (Izumida, 1995) or implanting materials such as penetrating hydrogels and urethane polymers in rats (Kurokawa et al., 2011; Yang et al., 2015), twisting plastic screws into the spinal canal of rabbits (Kanchiku et al., 2001), or constructing twy/twy transgenic mice with spontaneous atlantoaxial membrane ossification and cervical canal stenosis (Hirai et al., 2013). We have previously reported a stable, convenient and applicable method of establishing a chronic CSCI model that mimics clinical CCM by implanting a water-absorbable polyurethane polymer sheet into rat cervical canal (Yu et al., 2021). The neurologic behavior of CSCI rats reached its lowest at the 4th week and recovered to a stable status at the 8th week after persistent compression (Cheng et al., 2015). Thus, we selected the 4th and 8th weeks after compression as landmark time points of the deterioration phase and recovery phase respectively. We identified various pathological changes, including decreased microvascular density, blood-spinal cord barrier disruption and ischemia-hypoxia changes, at different time points following chronic CSCI (Long et al., 2012, 2015; Xu et al., 2017; Cheng et al., 2019; Yu et al., 2021). These pathologies can lead to oxidative stress-mediated neuronal and glial cell death inside the spinal parenchyma (Cheng et al., 2019). Nevertheless, the exact molecular mechanisms underlying the different stages of chronic CSCI remain unclear.

Ferroptosis is a new form of regulated cell death first reported by Dixon in 2012. It is an iron-dependent and caspase-independent form of cell death caused by toxic lipid peroxidation that leads to plasma membrane disruption and necrotic-like cell death (Chen et al., 2021b; Tang et al., 2021). This non-

[1]Department of Spine Surgery, Orthopedics Center of Guangdong Provincial People's Hospital (Guangdong Academy of Medical Sciences), Southern Medical University, Guangzhou, Guangdong Province, China; [2]Department of Spine Surgery, The First Affiliated Hospital, Sun Yat-sen University, Guangzhou, Guangdong Province, China; [3]Department of Gastroenterology, Guangzhou Women and Children's Medical Center, Jinan University, Guangzhou, Guangdong Province, China; [4]Department of Spine Surgery, Zhujiang Hospital, Southern Medical University, Guangzhou, Guangdong Province, China
*Correspondence to: Yang Duan, MD, PhD, duanxy@smu.edu.cn.
https://orcid.org/0000-0003-4809-9516 (Yang Duan)
#These authors contributed equally to this work.

How to cite this article: *Yu Z, Cheng X, Pan W, Yu C, Duan Y (2023) The ferroptosis activity is associated with neurological recovery following chronic compressive spinal cord injury. Neural Regen Res 18(11):2482-2488.*

apoptotic cell death is characterized by the iron-mediated triggering of lipid reactive oxygen species accumulation, which ultimately leads to cell death (Dixon et al., 2012). Ratan reviewed the chemical biology of ferroptosis and emphasized its pervasiveness in central nervous system damage (Ratan, 2020). Glutamate-induced ferroptosis may play crucial roles in oxidative-dominant central nervous system disorders, such as Alzheimer's disease, stroke, Parkinson's disease, and traumatic acute spinal cord injury (Do Van et al., 2016; Alim et al., 2019; Ashraf et al., 2020; Feng et al., 2021). Although ischemia- and peroxidation-induced neuronal cell death has also been frequently reported as a central pathophysiological feature of chronic CSCI, the role of ferroptosis in chronic CSCI has not been elucidated.

To understand the molecular mechanisms and role of ferroptosis in CCM progression, we analyzed the transcriptomic alterations and ferroptosis activity at different stages during chronic CSCI and identified key molecules that are differentially regulated at various stages of spinal cord compression.

Methods

Rat model of chronic spinal cord compression injury

Twenty-four adult (10 weeks old) female Sprague Dawley rats (250–280 g) were randomly allocated to sham (n = 8) and chronic CSCI (n = 16) groups (**Figure 1A**). Male rats have higher mortality rates than female rats after CSCI surgery owing to urinary tract infection and aggressiveness (Swartz et al., 2007), thus male rats were not included in this study. The rats in both groups were anesthetized with 1% pentobarbital (40 mg/kg) (Servicebio, Wuhan, China) and underwent C5 laminectomies. A polymer (1 × 3 × 1 mm^3) was implanted into the C6 epidural space on the posterolateral side of each rat in the chronic CSCI group (Yu et al., 2021). In the sham group, the polymer was inserted into the C6 epidural space in the same way but was removed 1 minute later. Following surgery, the incisions were closed in layers with complete hemostasis, and all rats were administered penicillin G (80 U/g) and carprofen (4–5 mg/kg, Pfizer, New York, NY, USA) to prevent infection and pain. After the surgery, the rats were provided free access to food and water and kept under the following conditions: temperature of 20–24°C, humidity of 40–50%, and a 12-hour light-dark cycle. This study was approved by the Institutional Review Board for Animal Experiments of Southern Medical University, Guangzhou, China (Ethic number: LAEC-2020-203) on December 25, 2020. All experiments were designed and reported according to the Animal Research: Reporting of *In Vivo* Experiments (ARRIVE) guidelines (Percie du Sert et al., 2020).

Behavior analysis and electrophysiological evaluations

The Basso, Beattie, and Bresnahan (BBB) locomotor scale (Basso et al., 1995) and inclined plane test (IPT) (Rivlin and Tator, 1977) were conducted before surgery and weekly postoperatively to evaluate motor functional changes. A BBB score of 0 indicates complete paralysis of the hind limbs and a full score of 21 indicates normal hind limb movement. Scores lower than 7 indicate isolated joint movements without hind limb movement, intermediate scores (8–13) indicate uncoordinated pace intervals, and scores higher than 14 indicate coordinated movements of the fore and hind limbs. The rats were placed on a wire-netting board for IPT. The plate was initially placed horizontally (0°), and the angle was increased by 5°–10° at each attempt. The maximum angle at which the rat remained on the plate for 10 seconds was recorded. Motor-evoked potentials (MEPs) and somatosensory-evoked potentials (SSEPs) (Nicolet Endeavor CR, San Diego, CA, USA) were measured twice per week to determine motor and somatosensory transduction deficits in the spinal cord, as described in our previous study (Yu et al., 2021). Reduced amplitudes and prolonged latencies of MEP and SSEP waves are hallmarks of conduction blockage. For severe conduction deficits, the target waves of MEP and SSEP can even be unrecognizable. The behavioral and neurophysiological assessments were conducted by two researchers who were blinded to the grouping.

RNA extraction and transcriptome sequencing

We performed RNA sequencing and analyzed the gene expression of spinal cord tissue samples from each group (sham, CSCI_4w, and CSCI_8w). Total RNA was extracted from the spinal cords (n = 3 or 4) of each group using a TransZol Up Plus RNA Kit (Servicebio). Polyadenylated mRNA isolation, second strand cDNA synthesis, and sequencing library preparation and purification were performed using the TruSeq® RNA Sample Preparation Kit v2 (Illumina, San Diego, CA, USA) and AMPure XP system (Beckman Coulter, Beverly, CA, USA). After library creation, transcriptome sequencing was carried out using the Illumina HiSeq 2500 platform (Illumina).

Data analysis for gene expression and enrichment analyses

At 4 and 8 weeks after CSCI, raw sequencing reads were filtered using Seqtk (https://github.com/lh3/seqtk) (Shen et al., 2016) and mapped using Hisat2 (http://daehwankimlab.github.io/hisat2/) (Kim et al., 2015) with the human GRCh38 genome reference. The R packages Stringtie (http://ccb.jhu.edu/software/stringtie/) (Pertea et al., 2016) and EdgeR were used to generate fragments per kilobase million values and to identify differentially expressed genes (DEGs), respectively. P-values in the multiple tests were set by the false discovery rate, and the fold changes were estimated according to the false discovery rate in each sample. Genes with expression value greater than 1.5-fold change and false discovery rate P-value < 0.05 were considered differentially expressed.

The Gene Ontology (GO) database (http://geneontology.org/) (Harris et al., 2004) was used for cell components, biological processes, and molecular function enrichment analyses. The Kyoto Encyclopedia of Genes and Genomes (KEGG) database (https://www.kegg.jp/) (Kanehisa and Goto, 2000) was used for pathway enrichment analysis. The ferroptosis-related genes were acquired via searching the GeneCards database (https://www.genecards.org/) (Stelzer et al., 2016) and FerrDb database (http://www.zhounan.org/ferrdb/) (Zhou and Bao, 2020) with "ferroptosis" as the keyword. The acquired genes of the two databases were merged, and the duplicates were removed. Finally, 470 ferroptosis genes were obtained. All the enrichment analyses were performed using the cluster Profiler (https://guangchuangyu.github.io/software/clusterProfiler/) (Yu et al., 2012).

Quantitative reverse transcription-polymerase chain reaction

At 4 and 8 weeks after CSCI, total RNA was isolated from the spinal cord samples using TRIZOL reagent (Thermo Fisher Scientific, Waltham, MA, USA). cDNA was synthesized using the PrimerScript RT Master Mix (RR036, Takara, Dalian, China) according to the manufacturer's instructions. Relative gene expression was detected using TB Green® Premix Ex Taq™ II (RR820A, Takara). The primer sequences used are listed in **Table 1**. Quantitative reverse transcription-polymerase chain reaction (qRT-PCR) was performed using the Applied Biosystems StepOnePlus system (Thermo Fisher Scientific). Relative mRNA expression was normalized to β-actin gene expression using the ΔCt method ($2^{-\Delta\Delta Ct}$) (Livak and Schmittgen, 2001).

Table 1 | **Primer sequences for quantitative reverse transcription-polymerase chain reaction**

Gene	Primer sequence (5'–3')
ARNTL (BMAL1)	F: CAT GCA ACG CAA TGT CCA G
	R: GTG TAT GGA TTG GTG GCA CCT
GPX4	F: GCC GAG TGT GGT TTA CGA ATC
	R: ACG CAG CCG TTC TTA TCA ATG
MafG	F: GTG TGA GTG CCT GCT CAC T
	R: AGG TGC TGG TTC AAC TCT CG
FAR1	F: GGC TGC GCT GAG ATT TGG
	R: GAA ACC AGT GGC TCC TGT GA
PTEN	F: ACC AGG ACC AGA GGA AAC CT
	R: CCT TGT CAT TAT CCG CAC GC
β-Actin	F: GAG ATT ACT GCT CTG GCT CCT A
	R: GGA CTC ATC GTA CTC CTG CTT G

GPX4: Glutathione peroxidase 4; *MafG*: MAF BZIP transcription factor G.

Malondialdehyde quantification assay

At 4 and 8 weeks after CSCI, malondialdehyde (MDA) levels in fresh spinal cord tissue from each group were evaluated with an MDA assay kit (S0131S, Beyotime, Shanghai, China) according to the manufacturer's instructions. Briefly, rat spinal cord tissue from each group was homogenized in 500 μL RIPA lysis buffer (Servicebio). The homogenates were centrifuged at 1073 × g for 10 minutes at 4°C, after which the supernatants were collected. Lipid peroxidation was assessed by quantifying the optical density of the colored complex formed by MDA and thiobarbituric acid reaction. The MDA level was presented as a relative ratio to the sham group.

Transmission electron microscopy

At 4 and 8 weeks after CSCI, rat spinal cord tissue (2 × 2 mm^2) from the C6 level of the lesioned side was harvested and fixed in 2.5% phosphate-buffered glutaraldehyde and 1% osmium tetroxide (Servicebio) for 48 hours. Tissue was sliced into 0.05-μm-thick sections using a pathology slicer (Shanghai Leica Instrument Co., Ltd., Shanghai, China), and carefully stained with uranium acetate and then lead citrate (Servicebio). Finally, sections from each group were imaged using a transmission electron microscope (Hitachi HT7700, Hitachi, Tokyo, Japan).

Tissue processing for histological and immunofluorescence analysis at 4 and 8 weeks after CSCI

At 4 and 8 weeks after CSCI, the rats in each group were anesthetized and perfused with 4% paraformaldehyde through the heart. C6 level spinal cord was harvested, fixed with 10% neutral buffered formaldehyde at 4°C for 1 week, and subsequently embedded in paraffin. These blocks were sliced into 5-μm-thick sections using a pathology slicer (Shanghai Leica Instrument Co., Ltd.) and stained with hematoxylin and eosin (H&E) (Servicebio). To evaluate the severity of histopathological injury, the images were scored based on the gray and white matter structure under a light microscope (Olympus, Tokyo, Japan) at 4× and 40× magnifications, according to a previously published method (Liu et al., 2014; Sun et al., 2022). Scoring was performed by two pathologists who were blinded to the experiment. Microscopic injuries include hemorrhage, cellular edema, necrosis, and neutrophil infiltration. The severity of the injuries was scored based on the area of the injuries, as follows: 0, no injury; 1, injury to 25% of the field; 2, injury to 55% of the field; 3, injury to 75% of the field; and 4, diffuse injury (Sun et al., 2022).

For immunofluorescence staining, the slides were placed in a microwave for epitope retrieval. The sections were permeabilized in 0.03% Triton X-100 for 30 minutes and then blocked with 5% bovine serum albumin (Solarbio, Beijing, China) for 30 minutes. Subsequently, they were incubated with

primary antibodies overnight at 4°C. The primary antibodies used were anti-GPX4 (a marker for anti-ferroptosis activity; mouse, 1:400, Proteintech, Rosemont, IL, USA, Cat# 67763-1-Ig, RRID: AB_2909469), anti-MafG (a marker for anti-ferroptosis activity; mouse, 1:150, Santa Cruz Biotechnology, Cat# sc-166548, RRID: AB_2137685), and anti-NeuN (a neuronal marker; rabbit, 1:150, Abcam, Cambridge, MA, USA, Cat# ab104225, RRID: AB_10711153). The next day, the sections were washed three times with phosphate-buffered saline (PBS) and subsequently incubated with secondary antibodies (Alexa Fluor® 488-conjugated goat anti-mouse IgG, 1:400, Servicebio, Cat# GB25301, RRID: AB_2904018 or Cy3-conjugated goat anti-rabbit IgG, 1:300, Servicebio, Cat# GB21303, RRID: AB_2861435) at room temperature for 60 minutes. Finally, the sections were incubated with 4′,6-diamidino-2-phenylindole (DAPI; Beyotime, Cat# C1005) for 20 minutes at 22–25°C. A fluorescence microscope (Leica DM 4P, Wetzlar, Germany) was used to observe the tissue sections. ImageJ software (version 1.0, National Institutes of Health, Bethesda, Maryland, USA; Schneider et al., 2012) was used to examine the fluorescence intensity.

Immunoprecipitation

At 4 and 8 weeks after CSCI, spinal cord tissue was homogenized in IGEPAL CA-630 buffer (Sigma-Aldrich, St. Louis, MO, USA, Cat# 9002-93-1). After centrifugation, the supernatant was subjected to immunoprecipitation with anti-Nrf2 (rabbit, 1:1000, Proteintech, Cat# 16396-1-AP, RRID: AB_2782956) at 4°C overnight. The samples were then incubated with immobilized antibody beads at 4°C for 2 hours. They were also subjected to immunoprecipitation with the IgG isotype control. Following immunoprecipitation and washing with PBS three times, the samples were eluted with glycine-HCl (0.1 M, pH 3.5), and the proteins were subsequently analyzed for Nrf2 and MafG using western blotting.

Western blot analysis

At 4 and 8 weeks after CSCI, the C6 spinal samples were extracted using RIPA lysis buffer (Servicebio). The protein levels were determined using the Bicinchoninic Acid Kit (Servicebio), according to the manufacturer's instructions. Following denaturation, the proteins were separated and transferred to polyvinylidene fluoride membranes (Millipore, Billerica, MA, USA). The membranes were blocked with 5% skim milk in PBS for 1 hour at room temperature and incubated with primary antibodies overnight at 4°C. The primary antibodies used in this study were anti-GPX4 (mouse, 1:2000, Proteintech, Cat# 67763-1-Ig, RRID: AB_2909469), anti-MafG (mouse, 1:500, Santa Cruz Biotechnology, Cat# sc-166548, RRID: AB_2137685), anti-α-tubulin (mouse, 1:5000, Proteintech, Cat# 66031-1-Ig, RRID: AB_11042766), and anti-Nrf2 (rabbit, 1:1000, Proteintech, Cat# 16396-1-AP, RRID: AB_2782956). The membranes were then washed and incubated with secondary antibodies (goat anti-mouse, 1:5000, Servicebio, Cat# GB23301, RRID: AB_2904020; and goat anti-rabbit, 1:5000, Servicebio, Cat# GB23303, RRID: AB_2811189) for 1 hour at room temperature. The proteins were imaged using electrogenerated chemiluminescence reagents (Servicebio), and the optical densities of the target bands were quantified with the AlphaEaseFC 4.0 imaging system (Alpha Innotech, San Leandro, CA, USA). For the quantitative analysis, the relative expressions were normalized to the optical density of the α-tubulin bands.

Statistical analysis

No statistical methods were used to predetermine sample sizes; however, our sample sizes were similar to those reported in a previous publication (Sun et al., 2022). Statistical analysis was performed using SPSS 25.0 (SPSS Inc., Chicago, IL, USA). Data are presented as the mean ± standard deviation. Student's *t*-test was performed to determine inter-group differences. The correlation analysis was performed using Spearman's or Pearson's correlation coefficients. *P*-values < 0.05 were considered statistically significant.

Results

Neurological functional changes following chronic CSCI

The BBB scores in the sham group were 21 points throughout the study. However, the BBB scores in the chronic CSCI group declined significantly after compression surgery compared with those in the sham group (**Figure 1C**; $P < 0.001$). The BBB scores in the chronic CSCI group reached their lowest values at 4 weeks. There was no significant difference in the BBB scores of the chronic CSCI group between 3 and 5 weeks; however, the scores were significantly improved after 6 weeks compared with those at 4 weeks (**Figure 1C**; $P < 0.05$). The IPT results demonstrated similar changes (**Figure 1D**). The neurophysiological examinations, including MEPs and SSEPs, also showed a similar trend in nerve conduction function. In the chronic CSCI group, the amplitudes of MEP ($P < 0.001$) and SSEP ($P < 0.001$) were significantly reduced compared with those in the sham group. The amplitudes were significantly improved (increased amplitude and shortened latency) at 8 weeks compared with those at 4 weeks in the chronic CSCI group ($P < 0.05$; **Figure 1E** and **F**). The study design and schematic of the chronic CSCI model are shown in **Figure 1A** and **B**, and demonstrate that our chronic CSCI rat model is compatible with the clinical CCM situation.

Tissue damage following chronic CSCI

The microstructure of the spinal cords stained with H&E was observed in each group at different magnifications. The spinal cords in the sham group were intact at different magnifications (**Figure 2A** and **B**). At low magnification, the extracellular matrix was degraded in the chronic CSCI group, leaving a large cavity in the spinal cord at 4 weeks after chronic compression. At high magnification, abnormal structure of the posterior funiculus and dorsal horn, prevalent edema, and neuronal nuclei fragmentation were observed. Some neurons changed to an elongated spindle shape owing to cytoplasmic loss; most of these were observed in the posterior horn (**Figure 2C** and **D**). At 8 weeks following chronic compression, although the spinal cord dorsal horn remained disordered, the spinal cord edema and inflammatory infiltration were significantly improved compared with those at week 4. The extracellular matrix was remodeled, and there appeared to be an increase of neurons and vessels (**Figure 2E** and **F**). As shown in **Figure 2G**, the histopathological scores of the chronic CSCI rats were at their highest at week 4 ($P < 0.001$) and had significantly decreased at week 8 ($P < 0.01$), indicating that the pathological damage was most severe in the middle of our observation period, and started resolving by the end of observation. Moreover, the histopathological scores of the rats were significantly negatively correlated with BBB scores ($R = –0.95$, $P < 0.001$; **Figure 2H**), demonstrating the histopathological and neurobehavioral consistency of this chronic CSCI model.

RNA sequencing and qRT-PCR validation following chronic CSCI

We performed comparisons between the sham, CSCI_4w, and CSCI_8w groups to identify DEGs (**Figure 3A**). The fragments per kilobase million distribution boxplot and mRNA expression heatmap obtained through hierarchical clustering analysis are shown in **Figure 3B** and **C**. The heatmap and principal component analysis map of mRNA expression indicated a high concordance between the sham, CSCI_4w, and CSCI_8w samples (**Figure 3C** and **D**). According to the criteria described in the Methods section, the 4- and 8-week compression results identified 510 and 864 DEGs, respectively, compared with the sham group. Of those, we sorted out 407 overlapping DEGs, including 205 upregulated and 202 downregulated genes (**Figure 3E–G**). All DEGs are listed in **Additional Tables 1** and **2**. We analyzed the 407 overlapping DEGs using GO and KEGG analyses. As shown in **Figure 3H–J**, the top functional enrichment included dopaminergic synapses, circadian entrainment, and ferroptosis activity. The KEGG pathway enrichment analysis of the integrated DEGs identified ferroptosis, presynapse, and postsynaptic membrane activities as the top three significantly enriched functional pathways at 4 weeks of compression. Dopaminergic synapse, ferroptosis, and adrenergic signaling activities were the top enriched pathways at 8 weeks of compression.

The dynamic changes in the ferroptosis-related DEGs between the sham, CSCI_4w, and CSCI_8w groups are shown in the heatmap and cluster dendrogram in **Figure 4**. Some of these genes were further validated using qRT-PCR. Compared with those in the sham group, ARNTL, GPX4, and MafG expression were significantly downregulated at 4 weeks and upregulated at 8 weeks in the CSCI groups. FAR1 and PTEN were only downregulated at 8 weeks after compression.

Ferroptosis is increased at 4 weeks after compression and reduced at 8 weeks

Given that the DEGs were related to ferroptosis, we used TEM to observe any ultrastructural changes in the neurons and to confirm the occurrence of ferroptosis. Compared with those in the sham group, the endoplasmic reticulum membranes and intracellular structures in the CSCI_4w and CSCI_8w groups were severely disrupted (**Figure 5A**, **D** and **G**). Compared with the normal mitochondria in the sham group, the mitochondria in the CSCI_4w group had noticeable morphological abnormalities, including smaller size, lack of cristae, swelling, and vacuoles (**Figure 5B**, **E** and **H**). These morphological changes are associated with ferroptosis (Chen et al., 2021a). In the CSCI_8w group, the mitochondrial abnormalities appeared to be improved, and mitochondrial swelling and vacuoles were ameliorated (**Figure 5C**, **F** and **I**). The MDA content in the spinal cord was significantly increased in the CSCI_4w group compared with the sham ($P < 0.001$) or CSCI_8w group ($P < 0.001$; **Figure 5J**). MDA level was significantly negatively correlated with BBB scores (rs = –0.88, $P < 0.001$; **Figure 5K**).These results indicated that oxidative damage in mitochondria and the ferroptosis activity peaked at 4 weeks and was attenuated at 8 weeks after chronic CSCI.

MafG and GPX4 expression suggests anti-ferroptosis activity in neurons during the later stages of chronic CSCI

GPX4 and MafG are master negative regulator genes of ferroptosis (Friedmann Angeli et al., 2014; Yang et al., 2014; Sun et al., 2016). We used immunofluorescence analysis to investigate the localization and expression of GPX4 and MafG in spinal cord cells. NeuN is a classical neuronal marker (Gusel'nikova and Korzhevskiy, 2015). Some $GPX4^+$ and $MafG^+$ neuronal cells were observed in the spinal cord sections of the sham group (**Figure 6A**). The number of $MafG^+/NeuN^+$ cells decreased sharply at 4 weeks ($P = 0.021$) and increased at 8 weeks ($P = 0.034$) after chronic CSCI, compared with that of the sham group. The number of GPX4+/NeuN+ cells showed a similar trend (Sham *vs.* CSCI_4w: $P = 0.042$; CSCI_4w *vs.* CSCI_8w: $P < 0.001$; **Figure 6B–E**).

Western blotting of GPX4 and MafG indicated similar changes; their expression was significantly decreased at week 4 and increased at week 8 following chronic CSCI, compared with that of the sham group (**Figure 7A** and **B**). GPX4 expression was positively correlated with MafG expression (Pearson correlation $r = 0.938$, $P < 0.001$; **Figure 7C**), suggesting that these two molecules may work together. Given that MafG mainly exerts its anti-ferroptosis activity by binding to transcription factors, such as Nrf2 (Motohashi et al., 2004), we used an immunoprecipitation assay and determined that the interaction between MafG and Nrf2 was attenuated at 4 weeks (sham *vs.* CSCI_4w, $P = 0.025$) and was significantly increased at 8 weeks (CSCI_4w *vs.* CSCI_8w, $P < 0.001$) of spinal cord compression (**Figure 7D** and **E**). The findings indicated that anti-ferroptosis activity was suppressed at 4 weeks and enhanced at 8 weeks after chronic CSCI.

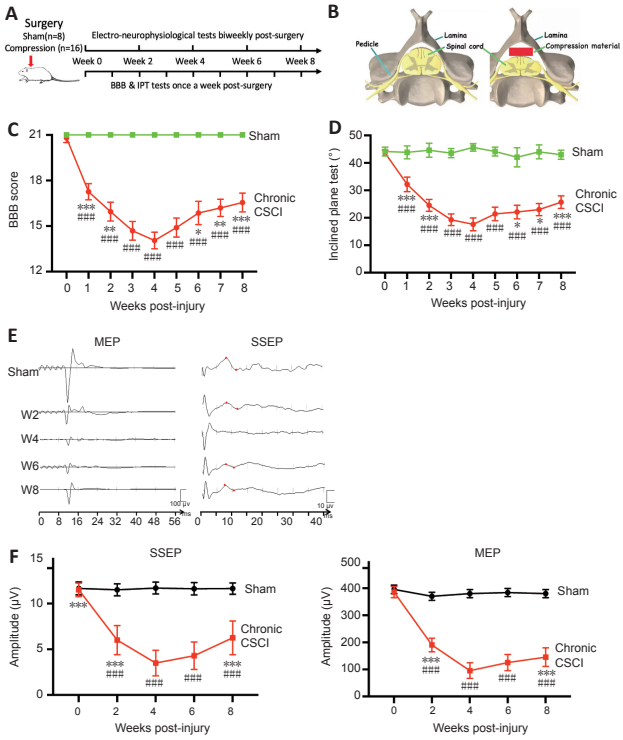

Figure 1 | Neurological functional changes following chronic CSCI.
(A) Study design: 24 adult, female Sprague-Dawley rats (250–280 g) were randomly allocated to sham (n = 8) and chronic CSCI (n = 16) groups. (B) Schematic images of the chronic CSCI model: a polymer was implanted inside the spinal canal to compress the spinal cord. (C, D) BBB scores (C) and IPT angles (D) in the sham and CSCI groups from weeks 1 to 8. (E, F) Representative images (E) and amplitude changes (F) of the MEPs and SSEPs from the sham and chronic CSCI group at different time points (weeks 2, 4, 6, and 8). $^{*}P < 0.05$, $^{**}P < 0.01$, $^{***}P < 0.001$, *vs.* week 4; $^{\#\#\#}P < 0.001$, *vs.* sham group (Student's *t*-test). Data are presented as mean ± SD. BBB: Basso, Beattie, and Bresnahan locomotor scale; IPT: inclined plane test; CSCI: chronic compressive spinal cord injury; MEP: motor evoked potentials; SSEP: somatosensory evoked potentials.

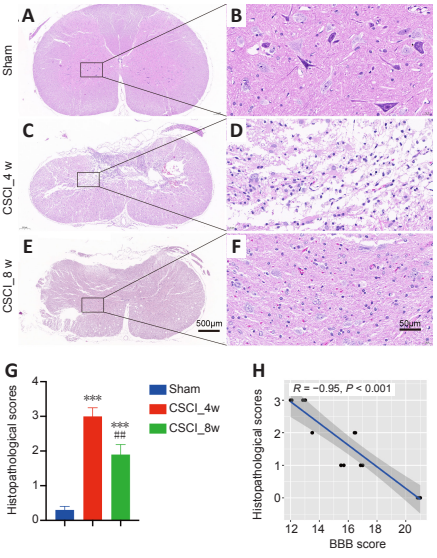

Figure 2 | Histology of spinal cord from the sham and chronic CSCI groups.
(A–F) Representative images of HE staining in the spinal cord of the sham (A, B) and chronic CSCI groups at 4 (C, D) and 8 weeks (E, F). (G) Histopathological scores. (H) Histopathological scores were significantly negatively correlated with BBB scores (Spearman correlation, R = −0.95, $P < 0.001$). Sample sizes: sham, n = 4; CSCI_4w, n = 4; and CSCI_8w, n = 4. Magnification: A–C, 4×; D–F, 40×. $^{***}P < 0.001$, *vs.* sham group; $^{\#\#}P < 0.01$, *vs.* CSCI_4w group (Student's *t*-test). Data are presented as the mean ± standard deviation in G. BBB: Basso, Beattie, and Bresnahan locomotor scale; CSCI: chronic compressive spinal cord injury; HE staining: hematoxylin and eosin staining.

Discussion

In the present study, we established a clinically relevant CCM model in rats and demonstrated that ferroptosis activity peaked at 4 weeks and was attenuated at 8 weeks during chronic compression. The ferroptosis activity was negatively correlated with the trend of functional neurophysiological changes, suggesting it has detrimental effects on neurological functional

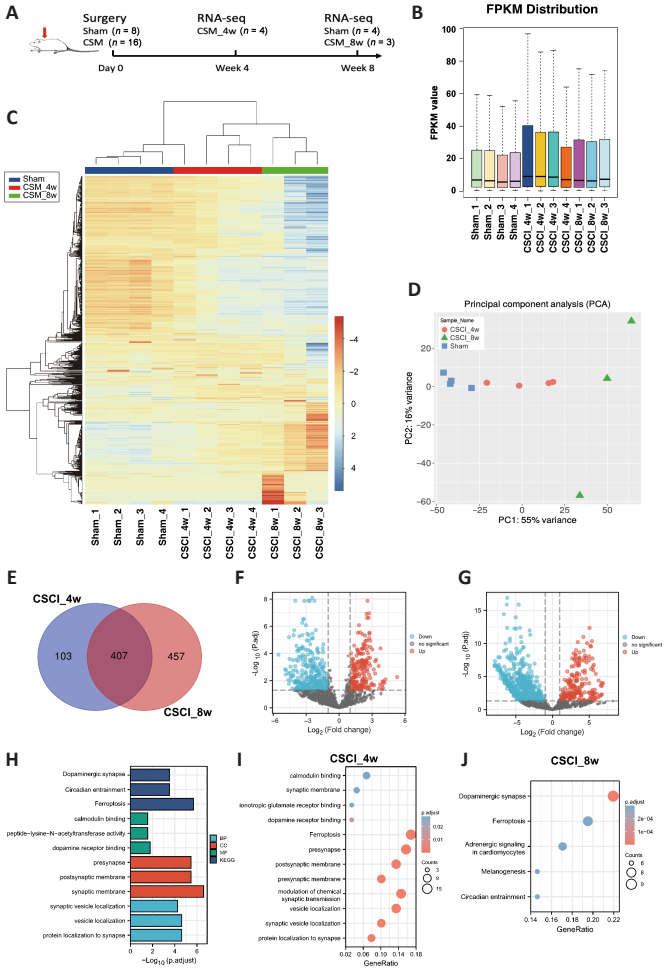

Figure 3 | Differential gene expression analysis of sham *vs.* CSCI_4w and CSCI_8w identified many genes induced upon chronic CSCI.
(A) Study design. (B) Boxplots of the FPKM values of all the samples (sham, n = 4; CSCI_4w, n = 4; CSCI_8w, n = 3). (C) Heatmap of the genes in the sham *vs.* CSCI_4w *vs.* CSCI_8w groups. (D) Principal component analysis to demonstrate the source of variance in our data. (E) Venn diagrams show the significantly differentially expressed genes between the sham and CSCI_4w or CSCI_8w groups. (F, G) Volcano plot and heatmap of the comparisons between the sham and CSCI_4w groups. (H) Gene ontology (GO) and Kyoto Encyclopedia of Genes and Genomes (KEGG) analyses of the compression time-dependent genes suggested a vital role of synaptic activity and localization in classifying chronic CSCI rats. (I, J) KEGG pathway analysis of the differentially expressed genes in the CSCI_4w group (I) and CSCI_8w group (J). The bubble color shading indicates the P values (stronger shading indicates a lower P value), and the bubble size indicates the frequency of the KEGG pathways. CSCI: Chronic compressive spinal cord injury.

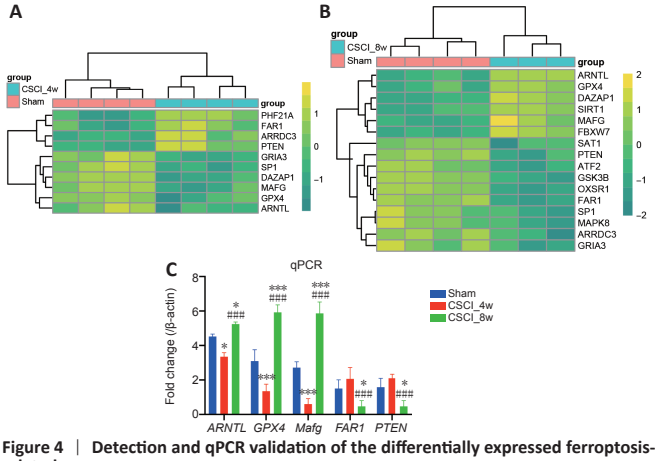

Figure 4 | Detection and qPCR validation of the differentially expressed ferroptosis-related genes.
(A, B) Heatmaps of the top differentially expressed genes related to ferroptosis from RNA sequencing in the CSCI_4w (A) and CSCI_8w groups (B). The color scale indicates the relative gene expression level. (C) Quantitative reverse transcription-polymerase chain reaction validations of the differentially expressed genes characterized by RNA sequencing. $^{*}P < 0.05$, $^{***}P < 0.001$, *vs.* sham group; $^{\#\#\#}P < 0.001$, *vs.* CSCI_4w group (Student's *t*-test). Sample size: sham, n = 4; CSCI_4w, n = 4; CSCI_8w, n = 3. ARNTL, GPX4, MafG, FAR1, PTEN were the top differentially expressed ferroptosis-related genes. ARNTL: Aryl hydrocarbon receptor nuclear translocator-like protein 1; FAR1: fatty acyl-CoA reductase 1; GPX4: glutathione peroxidase 4; MafG: MAF BZIP transcription factor G; PTEN: phosphatase and tensin homolog; qPCR: quantitative polymerase chain reaction.

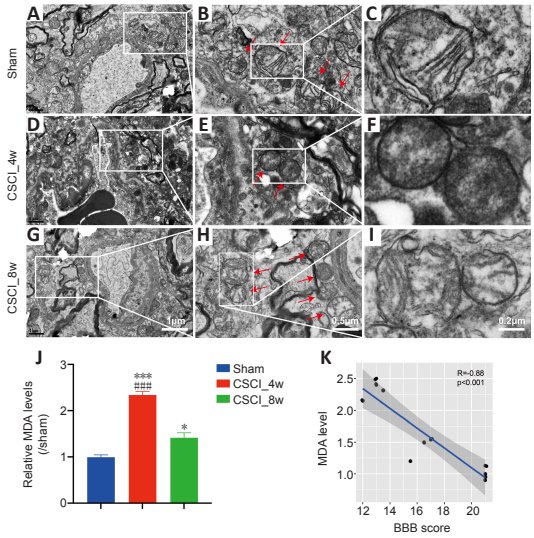

Figure 5 | Ferroptosis-specific mitochondrial changes and MDA accumulation levels after chronic CSCI.

(A–I) Representative transmission electron microscopy images of neurons and neuronal mitochondria in the sham (A–C), CSCI_4w (D–F), and CSCI_8w (G–I) groups. Red arrows indicate mitochondria. Ferroptosis-specific changes, including shrunken mitochondria, increased membrane density, and occasionally disrupted outer membranes, were evident in the CSCI_4w group (F). (J) MDA content in the spinal cord was significantly increased at 4 weeks after chronic CSCI, and attenuated at 8 weeks. *$P < 0.05$, ***$P < 0.001$, *vs.* sham group; ###$P < 0.001$, *vs.* CSCI_8w group (Student's *t*-test). Data are presented as the mean ± standard deviation. (K) MDA level was significantly negatively correlated with BBB scores (Spearman correlation, $R = -0.88$, $P < 0.001$). Sample sizes: Sham, $n = 4$; CSCI_4w, $n = 4$; and CSCI_8w, $n = 4$. MDA: Malondialdehyde; CSCI: compressive spinal cord injury.

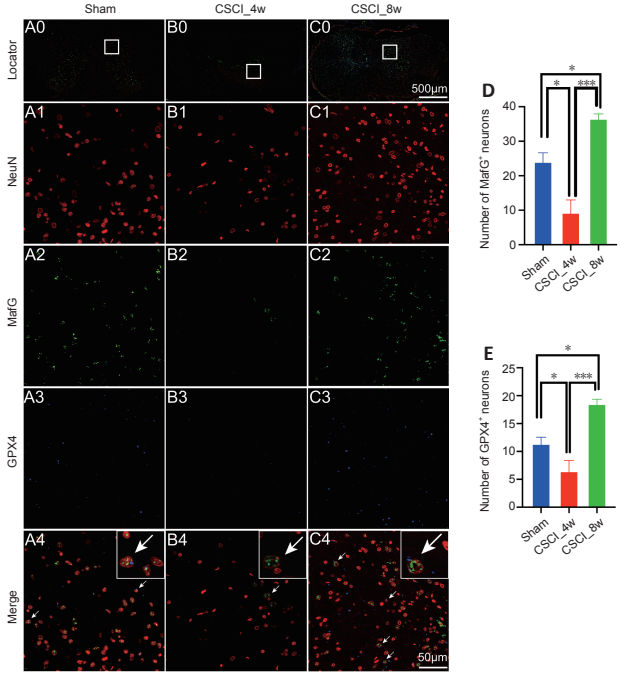

Figure 6 | IF of MafG and GPX4 in neurons after chronic CSCI.

(A0–C0) Overview images indicating the location of the magnified IF images. (A1–3 to C1–3) Magnified IF images stained with NeuN (A1–C1, red), MafG (A2–C2, green), GPX4 (A3–C3, blue) and merged channels (A4–C4). The white arrows indicate NeuN$^+$/MafG$^+$/GPX4$^+$ triple-labeled cells. NeuN and GPX4 are located in the cytoplasm of neuronal cells, whereas MafG primarily resides in the nuclei. (D, E) Numbers of MafG$^+$ and GPX4$^+$ neurons in each group. *$P < 0.05$, ***$P < 0.001$ (Student's *t*-test). Sample sizes: sham, $n = 4$; CSCI_4w, $n = 4$; and CSCI_8w, $n = 4$. Data are presented as the mean ± standard deviation. CSCI: Compressive spinal cord injury; IF: immunofluorescence; MafG: MAF BZIP transcription factor G; GPX4: glutathione peroxidase 4.

recovery. We also observed that expression of the anti-ferroptosis molecules GPX4 and MafG were decreased at 4 weeks and increased at 8 weeks. The MafG-Nrf2 interaction showed the same trend. To the best of our knowledge, this is the first study to analyze the transcriptomic changes and ferroptosis activity of chronic CSCI rats at different time points in an 8-week period. Our study suggests a relationship between ferroptosis and neurological damage

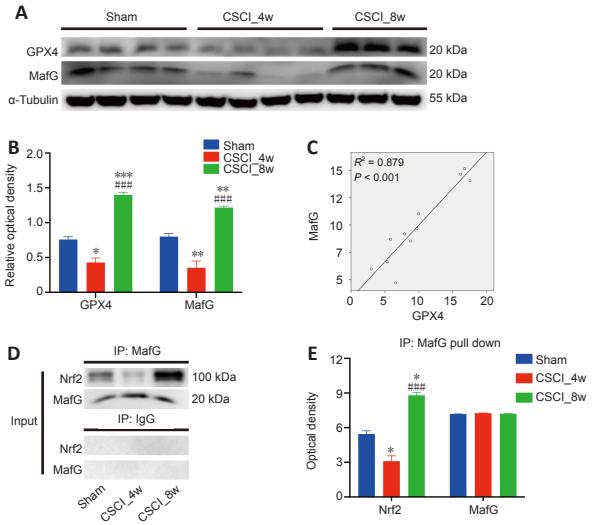

Figure 7 | Correlation between GPX4 and MafG expression, and the MafG-Nrf2 interaction after chronic CSCI.

(A, B) Western blotting of GPX4 and MafG was significantly decreased at week 4 but increased at week 8 following chronic CSCI, compared with that of the sham group. (C) Pearson correlation analysis indicated a significant positive correlation between MafG and GPX4 expression ($R^2 = 0.879$; $P < 0.001$). (D, E) Immunoprecipitation (IP) assay demonstrating the interaction between MafG and Nrf2, which was attenuated at 4 weeks and significantly increased at 8 weeks following spinal cord compression. *$P < 0.05$, **$P < 0.01$, *vs.* sham group; ###$P < 0.001$, *vs.* CSCI_4w group (Student's *t*-test). Data are presented as the mean ± standard deviation in B and E. Sample sizes: sham, $n = 4$; CSCI_4w, $n = 4$; and CSCI_8w, $n = 3$. CSCI: Compressive spinal cord injury; GPX4: Glutathione peroxidase 4; MafG: MAF BZIP transcription factor G; Nrf2: nuclear factor erythroid 2-related factor 2.

during CSCI, and provides new insights into the potential of anti-ferroptosis therapy in the treatment of CCM.

Similar to previous studies (Cheng et al., 2019, 2021; Yu et al., 2021), the BBB scores and neurophysiological measures reached their lowest values at 4 weeks after chronic spinal cord compression, and gradually recovered in the later stage, from weeks 4–8. The histopathological scores also showed the greatest damage at 4 weeks and were significantly correlated with BBB scores in rats with chronic CSCI. The results from this study confirmed that the implantation of a water-absorbable compressor made from polyurethane polymer in rats establishes a successful CCM model with consistent neurobehavioral and histopathological changes (Cheng et al., 2015, 2021; Yu et al., 2021). Moreover, the finding of the intrinsic self-repair capacity motivated us to explore the potential underlying mechanisms.

To date, the molecular mechanisms of the functional changes in a spinal cord following consistent compression have not been established. Only one study (Zhang et al., 2018a) used a Clariom D Rat GeneChip array to identify the differentially expressed lncRNAs, mRNAs, and pre-miRNAs in chronic CSCI rat models at 4 weeks after compression. However, the genechip array can only detect genes by known probe sequences. High-throughput sequencing, in contrast, does not need the construction of a probe library and data analysis is conducted on a mature bioinformatics platform that is more comprehensive and avoids subcloning errors, which produces more accurate results (Hurd and Nelson, 2009). Moreover, the authors (Zhang et al., 2018a) did not identify any significant biological pathway changes after the spinal cord compression, nor did they include data longer than 4 weeks after compression. In the present study, we firstly identified DEGs in the spinal cord after 4 and 8 weeks of compression compared with the sham group using high-throughput RNA sequencing. By comparing the 510 and 863 DEGs at the 4- and 8-week time points and using functional enrichment analyses, we found that ferroptosis, synaptic transmission activity, and neuronal signaling pathways are the most crucial biological pathways regulating the process of chronic CSCI.

Previous studies have reported that ferroptosis plays a vital role in secondary injury following acute traumatic SCI, and inhibitors, such as deferoxamine and SRS 16-86, promote motor functional recovery in SCI rats by inhibiting ferroptosis (Yao et al., 2019; Zhang et al., 2019). Ferroptosis also mediates selective motor neuron death in amyotrophic lateral sclerosis (Wang et al., 2022) and neurodegenerative disorders such as Parkinson's disease (Bellinger et al., 2011). However, the effects and role of ferroptosis in chronic CSCI remain unclear. In this study, TEM results confirmed that the severity of ferroptosis-specific mitochondrial changes, including shrunken mitochondria, increased membrane density, and occasionally disrupted outer membranes, reached its peak at 4 weeks and was partially alleviated at 8 weeks following CSCI. Furthermore, MDA levels were increased at 4 weeks and were attenuated at 8 weeks following chronic CSCI, and were negatively correlated with motor behavioral scores. Because MDA is a sensitive marker for lipid peroxidase and ferroptosis (Ohkawa et al., 1979; Chen et al., 2022), our results suggest that ferroptosis may exert negative effects on neurological recovery after chronic CSCI.

We also evaluated the expression of the ferroptosis markers GPX4 and MafG using semi-quantitative immunofluorescence and quantitative western blotting. Both proteins were significantly reduced at 4 weeks and greatly increased at 8 weeks following CSCI. We also observed a significant increase in the interaction between MafG and Nrf2 during the later stages of chronic CSCI via an immunoprecipitation assay. GPX4 is a selenocysteine-containing enzyme that counters lipid peroxide formation and is considered the master negative regulator of ferroptosis in cells (Friedmann Angeli et al., 2014; Yang et al., 2014). Depletion of GPX4 is associated with vulnerable neurons in Parkinson's disease (Bellinger et al., 2011), stroke (Zhang et al., 2018b), and acute spinal cord injury (Chen et al., 2020). In contrast, GPX4 overexpression effectively restored the ferroptosis defense, inhibited lipid peroxidation and motor neuron death, and improved motor function and outcomes in an amyotrophic lateral sclerosis model (Wang et al., 2022). Small musculoaponeurotic fibrosarcoma oncogene homolog (Maf) proteins, including MafF, MafG, and MafK, possess a basic leucine zipper (bZip) domain that interacts with other bZip transcription factors such as Nrf2 (Motohashi et al., 2004). Under oxidative stress or ischemic conditions, MafG binds to the Nrf2 protein and initiates a cascade reaction that includes nuclear translocation, transcriptional coactivators binding to antioxidant response elements, and target gene expression. These reactions activate anti-apoptosis and anti-ferroptosis pathways (Suzuki et al., 2013; Sun et al., 2016). Together, these results indicated that the anti-ferroptosis pathway in our model was suppressed at 4 weeks and activated at 8 weeks after chronic CSCI.

We further investigated the correlation between GPX4 and MafG expression following chronic CSCI. GPX4 and MafG expressions were decreased at 4 weeks and increased at 8 weeks following chronic CSCI, and were positively correlated with one another. The upregulation of protective GPX4 and MafG was consistent with our TEM findings of ferroptosis alleviation and neurological functional recovery. GPX4 and MafG (Sun et al., 2016) have been reported to exert their anti-ferroptosis effects in different pathways, and cross-talk between the two molecules has not been reported (Chen et al., 2020). Our findings suggest that the activation of anti-ferroptosis pathways likely plays a vital role in functional nerve recovery during the late stages of chronic CSCI.

Our study has certain limitations. First, this was an observational study. Although we did perform neurophysiological tests, transcriptional analysis of DEGs, TEM, and molecular validation assays, we did not perform gain-of-function or loss-of-function experiments. Further research is required to investigate the mechanisms by which these proteins influence each other as well as neurological functions. Second, the exact molecular mechanism by which these DEGs influence ferroptosis at different time points in chronic CSCI has not been clarified and further studies are required. Third, male rats were excluded from this study because of their high mortality rate owing to urinary tract infections and aggressiveness after chronic CSCI (Palacios et al., 2022). Further studies involving rats of both sexes are required to avoid sex bias.

In summary, our study determined the genome-wide expression profile of a consistently compressed rat spinal cord at different time points. Our findings suggest that the suppression of ferroptosis and the activation of several anti-ferroptosis-related genes, including GPX4 and MafG, may be involved in the process of spontaneous neurological recovery during the later stages of chronic CSCI. Our results provide a better understanding of the molecular mechanism underlying chronic CSCI and may help identify new therapeutic targets for CCM.

Author contributions: *ZY and XC drafted the manuscript. WP performed molecular experiments and collected the data. CY contributed to the animal experiments and revised the manuscript. YD made substantial contributions to the conception and design of the research. All authors gave final approval of the version to be published.*
Conflicts of interest: *The authors declare that they have no competing interests.*
Data availability statement: *All data generated or analyzed during this study are included in this published manuscript and its Additional files.*

Editor's evaluation: *This paper presents the molecular mechanisms and the role of ferroptosis in the progression of CCM, uncovers the transcriptomic alterations during chronic CSCI at different stages, especially at 4 and 8 weeks. It is a topic of interest to the researchers in the related areas. The study was well-designed and carried out with a scientific discipline, with a reasonable narrative and multiple ways of verification.*
Additional files:
Additional Table 1: *Differentially expressed genes identified in this study (CSCI_4w vs. sham).*
Additional Table 2: *Differentially expressed genes identified in this study (CSCI_8w vs. sham).*

References

Alim I, Caulfield JT, Chen Y, Swarup V, Geschwind DH, Ivanova E, Seravalli J, Ai Y, Sansing LH, Ste Marie EJ, Hondal RJ, Mukherjee S, Cave JW, Sagdullaev BT, Karuppagounder SS, Ratan RR (2019) Selenium drives a transcriptional adaptive program to block ferroptosis and treat stroke. Cell 177:1262-1279 e1225.

Ashraf A, Jeandriens J, Parkes HG, So PW (2020) Iron dyshomeostasis, lipid peroxidation and perturbed expression of cystine/glutamate antiporter in Alzheimer's disease: Evidence of ferroptosis. Redox Biol 32:101494.

Badhiwala JH, Ahuja CS, Akbar MA, Witiw CD, Nassiri F, Furlan JC, Curt A, Wilson JR, Fehlings MG (2020) Degenerative cervical myelopathy- update and future directions. Nat Rev Neurol 16:108-124.

Basso DM, Beattie MS, Bresnahan JC (1995) A sensitive and reliable locomotor rating scale for open field testing in rats. J Neurotrauma 12:1-21.

Bellinger FP, Bellinger MT, Seale LA, Takemoto AS, Raman AV, Miki T, Manning-Bog AB, Berry MJ, White LR, Ross GW (2011) Glutathione peroxidase 4 is associated with neuromelanin in substantia nigra and dystrophic axons in putamen of Parkinson's brain. Mol Neurodegener 6:8.

Chen X, Comish PB, Tang D, Kang R (2021a) Characteristics and biomarkers of ferroptosis. Front Cell Dev Biol 9:637162.

Chen X, Li J, Kang R, Klionsky DJ, Tang D (2021b) Ferroptosis: machinery and regulation. Autophagy 17:2054-2081.

Chen Y, Liu S, Li J, Li Z, Quan J, Liu X, Tang Y, Liu B (2020) The latest view on the mechanism of ferroptosis and its research progress in spinal cord injury. Oxid Med Cell Longev 2020:6375938.

Chen YX, Zuliyaer T, Liu B, Guo S, Yang DG, Gao F, Yu Y, Yang ML, Du LJ, Li JJ (2022) Sodium selenite promotes neurological function recovery after spinal cord injury by inhibiting ferroptosis. Neural Regen Res 17:2702-2709.

Cheng X, Yu Z, Xu J, Quan D, Long H (2021) Pathophysiological changes and the role of Notch-1 activation after decompression in a compressive spinal cord injury rat model. Front Neurosci 15:579431. Erratum in: Front Neurosci 15:665669.

Cheng X, Long H, Chen W, Xu J, Huang Y, Li F (2015) Three-dimensional alteration of cervical anterior spinal artery and anterior radicular artery in rat model of chronic spinal cord compression by micro-CT. Neurosci Lett 606:106-112.

Cheng X, Long H, Chen W, Xu J, Wang X, Li F (2019) The correlation between hypoxia-inducible factor-1alpha, matrix metalloproteinase-9 and functional recovery following chronic spinal cord compression. Brain Res 1718:75-82.

Dixon SJ, Lemberg KM, Lamprecht MR, Skouta R, Zaitsev EM, Gleason CE, Patel DN, Bauer AJ, Cantley AM, Yang WS, Morrison B, 3rd, Stockwell BR (2012) Ferroptosis: an iron-dependent form of nonapoptotic cell death. Cell 149:1060-1072.

Do Van B, Gouel F, Jonneaux A, Timmerman K, Gele P, Petrault M, Bastide M, Laloux C, Moreau C, Bordet R, Devos D, Devedjian JC (2016) Ferroptosis, a newly characterized form of cell death in Parkinson's disease that is regulated by PKC. Neurobiol Dis 94:169-178.

Feng Z, Min L, Chen H, Deng W, Tan M, Liu H, Hou J (2021) Iron overload in the motor cortex induces neuronal ferroptosis following spinal cord injury. Redox Biol 43:101984.

Friedmann Angeli JP, Schneider M, Proneth B, Tyurina YY, Tyurin VA, Hammond VJ, Herbach N, Aichler M, Walch A, Eggenhofer E, Basavarajappa D, Rådmark O, Kobayashi S, Seibt T, Beck H, Neff F, Esposito I, Wanke R, Förster H, Yefremova O, et al. (2014) Inactivation of the ferroptosis regulator Gpx4 triggers acute renal failure in mice. Nat Cell Biol 16:1180-1191.

Gusel'nikova VV, Korzhevskiy DE (2015) NeuN as a neuronal nuclear antigen and neuron differentiation marker. Acta Naturae 7:42-47.

Harris MA, Clark J, Ireland A, Lomax J, Ashburner M, Foulger R, Eilbeck K, Lewis S, Marshall B, Mungall C, Richter J, Rubin GM, Blake JA, Bult C, Dolan M, Drabkin H, Eppig JT, Hill DP, Ni L, Ringwald M, et al. (2004) The Gene Ontology (GO) database and informatics resource. Nucleic Acids Res 32(Database issue):D258-261.

Hirai T, Uchida K, Nakajima H, Guerrero AR, Takeura N, Watanabe S, Sugita D, Yoshida A, Johnson WE, Baba H (2013) The prevalence and phenotype of activated microglia/macrophages within the spinal cord of the hyperostotic mouse (twy/twy) changes in response to chronic progressive spinal cord compression: implications for human cervical compressive myelopathy. PLoS One 8:e64528.

Hurd PJ, Nelson CJ (2009) Advantages of next-generation sequencing versus the microarray in epigenetic research. Brief Funct Genomic Proteomic 8:174-183.

Izumida M (1995) A chronic spinal cord compression model in a rat with a 354A tumor. Nihon Seikeigeka Gakkai Zasshi 69:977-991.

Kanchiku T, Taguchi T, Kaneko K, Yonemura H, Kawai S, Gondo T (2001) A new rabbit model for the study on cervical compressive myelopathy. J Orthop Res 19:605-613.

Kanehisa M, Goto S (2000) KEGG: kyoto encyclopedia of genes and genomes. Nucleic Acids Res 28:27-30.

Kim D, Langmead B, Salzberg SL (2015) HISAT: a fast spliced aligner with low memory requirements. Nat Methods 12:357-360.

Kurokawa R, Murata H, Ogino M, Ueki K, Kim P (2011) Altered blood flow distribution in the rat spinal cord under chronic compression. Spine (Phila Pa 1976) 36:1006-1009.

Liu X, Zhou Y, Wang Z, Yang J, Gao C, Su Q (2014) Effect of VEGF and CX43 on the promotion of neurological recovery by hyperbaric oxygen treatment in spinal cord-injured rats. Spine J 14:119-127.

Livak KJ, Schmittgen TD (2001) Analysis of relative gene expression data using real-time quantitative PCR and the 2(-Delta Delta C(T)) Method. Methods 25:402-408.

Long HQ, Li GS, Hu Y, Wen CY, Xie WH (2012) HIF-1alpha/VEGF signaling pathway may play a dual role in secondary pathogenesis of cervical myelopathy. Med Hypotheses 79:82-84.

Long HQ, Li GS, Cheng X, Xu JH, Li FB (2015) Role of hypoxia-induced VEGF in blood-spinal cord barrier disruption in chronic spinal cord injury. Chin J Traumatol 18:293-295.

Motohashi H, Katsuoka F, Engel JD, Yamamoto M (2004) Small Maf proteins serve as transcriptional cofactors for keratinocyte differentiation in the Keap1-Nrf2 regulatory pathway. Proc Natl Acad Sci U S A 101:6379-6384.

Ohkawa H, Ohishi N, Yagi K (1979) Assay for lipid peroxides in animal tissues by thiobarbituric acid reaction. Anal Biochem 95:351-358.

Palacios JL, Luquin S, Quintanar JL, Munoz A (2022) Continuous administration of leuprolide acetate improves urinary function in male rats with severe thoracic spinal cord injury. Life Sci 310:121113.

Percie du Sert N, Hurst V, Ahluwalia A, Alam S, Avey MT, Baker M, Browne WJ, Clark A, Cuthill IC, Dirnagl U, Emerson M, Garner P, Holgate ST, Howells DW, Karp NA, Lazic SE, Lidster K, MacCallum CJ, Macleod M, Pearl EJ, et al. (2020) The ARRIVE guidelines 2.0: Updated guidelines for reporting animal research. PLoS Biol 18:e3000410.

Pertea M, Kim D, Pertea GM, Leek JT, Salzberg SL (2016) Transcript-level expression analysis of RNA-seq experiments with HISAT, StringTie and Ballgown. Nat Protoc 11:1650-1667.

Ratan RR (2020) The chemical biology of ferroptosis in the central nervous system. Cell Chem Biol 27:479-498.

Rivlin AS, Tator CH (1977) Objective clinical assessment of motor function after experimental spinal cord injury in the rat. J Neurosurg 47:577-581.

Schneider CA, Rasband WS, Eliceiri KW (2012) NIH Image to ImageJ: 25 years of image analysis. Nat Methods 9:671-675.

Shen W, Le S, Li Y, Hu F (2016) SeqKit: A cross-platform and ultrafast toolkit for FASTA/Q file manipulation. PLoS One 11:e0163962.

Stelzer G, Rosen N, Plaschkes I, Zimmerman S, Twik M, Fishilevich S, Stein TI, Nudel R, Lieder I, Mazor Y, Kaplan S, Dahary D, Warshawsky D, Guan-Golan Y, Kohn A, Rappaport N, Safran M, Lancet D (2016) The GeneCards suite: from gene data mining to disease genome sequence analyses. Curr Protoc Bioinformatics 54:1 30 31-31 30 33.

Sun X, Ou Z, Chen R, Niu X, Chen D, Kang R, Tang D (2016) Activation of the p62-Keap1-NRF2 pathway protects against ferroptosis in hepatocellular carcinoma cells. Hepatology 63:173-184.

Sun ZC, Liang F, Yang J, Hai Y, Su QJ, Liu XH (2022) The mechanism by which hyperbaric oxygen treatment alleviates spinal cord injury: genome-wide transcriptome analysis. Neural Regen Res 17:2737-2742.

Suzuki T, Motohashi H, Yamamoto M (2013) Toward clinical application of the Keap1-Nrf2 pathway. Trends Pharmacol Sci 34:340-346.

Swartz KR, Fee DB, Joy KM, Roberts KN, Sun S, Scheff NN, Wilson ME, Scheff SW (2007) Gender differences in spinal cord injury are not estrogen-dependent. J Neurotrauma 24:473-480.

Tang D, Chen X, Kang R, Kroemer G (2021) Ferroptosis: molecular mechanisms and health implications. Cell Res 31:107-125.

Wang T, Tomas D, Perera ND, Cuic B, Luikinga S, Viden A, Barton SK, McLean CA, Samson AL, Southon A, Bush AI, Murphy JM, Turner BJ (2022) Ferroptosis mediates selective motor neuron death in amyotrophic lateral sclerosis. Cell Death Differ 29:1187-1198.

Xu J, Long H, Chen W, Cheng X, Yu H, Huang Y, Wang X, Li F (2017) Ultrastructural features of neurovascular units in a rat model of chronic compressive spinal cord injury. Front Neuroanat 11:136.

Yang T, Wu L, Wang H, Fang J, Yao N, Xu Y (2015) Inflammation level after decompression surgery for a rat model of chronic severe spinal cord compression and effects on ischemia-reperfusion injury. Neurol Med Chir (Tokyo) 55:578-586.

Yang WS, SriRamaratnam R, Welsch ME, Shimada K, Skouta R, Viswanathan VS, Cheah JH, Clemons PA, Shamji AF, Clish CB, Brown LM, Girotti AW, Cornish VW, Schreiber SL, Stockwell BR (2014) Regulation of ferroptotic cancer cell death by GPX4. Cell 156:317-331.

Yao X, Zhang Y, Hao J, Duan HQ, Zhao CX, Sun C, Li B, Fan BY, Wang X, Li WX, Fu XH, Hu Y, Liu C, Kong XH, Feng SQ (2019) Deferoxamine promotes recovery of traumatic spinal cord injury by inhibiting ferroptosis. Neural Regen Res 14:532-541.

Yu G, Wang LG, Han Y, He QY (2012) clusterProfiler: an R package for comparing biological themes among gene clusters. OMICS 16:284-287.

Yu Z, Cheng X, Chen J, Huang Z, He S, Hu H, Lin S, Zou Z, Huang F, Chen B, Wan Y, Peng X, Zou X (2021) Spinal cord parenchyma vascular redistribution underlies hemodynamic and neurophysiological changes at dynamic neck positions in cervical spondylotic myelopathy. Front Neuroanat 15:729482.

Zhang L, Yang L, Li W, Yang Y, Sun W, Gong P, Wang L, Wang K (2018a) A potential competitive endogenous RNA pathway involved in chronic spinal cord injury. Med Sci Monit 24:8022-8032.

Zhang Y, Sun C, Zhao C, Hao J, Zhang Y, Fan B, Li B, Duan H, Liu C, Kong X, Wu P, Yao X, Feng S (2019) Ferroptosis inhibitor SRS 16-86 attenuates ferroptosis and promotes functional recovery in contusion spinal cord injury. Brain Res 1706:48-57.

Zhang Z, Wu Y, Yuan S, Zhang P, Zhang J, Li H, Li X, Shen H, Wang Z, Chen G (2018b) Glutathione peroxidase 4 participates in secondary brain injury through mediating ferroptosis in a rat model of intracerebral hemorrhage. Brain Res 1701:112-125.

Zhou N, Bao J (2020) FerrDb: a manually curated resource for regulators and markers of ferroptosis and ferroptosis-disease associations. Database (Oxford) 2020:baaa021.

C-Editor: Zhao M; S-Editor: Li CH; L-Editors: Li CH, Song LP; T-Editor: Jia Y